Published in final edited form as:
Nat Med. 2012 June ; 18(6): 967–973. doi:10.1038/nm.2759.

ApoB-containing lipoproteins regulate angiogenesis by modulating expression of VEGF receptor 1

Inbal Avraham-Davidi[1], **Yona Ely**[1], **Van N Pham**[2], **Daniel Castranova**[2], **Moshe Grunspan**[1], **Guy Malkinson**[1], **Liron Gibbs-Bar**[1], **Oded Mayseless**[1], **Gabriella Allmog**[1], **Brigid Lo**[2], **Carmen M Warren**[3], **Tom T Chen**[3], **Josette Ungos**[2,9], **Kameha Kidd**[2,9], **Kenna Shaw**[2,9], **Ilana Rogachev**[4], **Wuzhou Wan**[5], **Philip M Murphy**[5], **Steven A Farber**[6], **Liran Carmel**[7], **Gregory S Shelness**[8], **M Luisa Iruela-Arispe**[3], **Brant M Weinstein**[2], and **Karina Yaniv**[1]

[1]Department of Biological Regulation, Weizmann Institute of Science, Rehovot, Israel

[2]Laboratory of Molecular Genetics, National Institute of Child Health and Human Development, National Institutes of Health, Bethesda, Maryland, USA

[3]Department of Molecular, Cell and Developmental Biology, University of California Los Angeles, Los Angeles, California, USA

[4]Department of Plan Sciences, Weizmann Institute of Science, Rehovot, Israel

[5]Laboratory of Molecular Immunology, National Institute of Allergy and Infectious Diseases, National Institutes of Health, Bethesda, Maryland, USA

[6]Department of Embryology, Carnegie Institution for Science, Baltimore, Maryland, USA

[7]Department of Genetics, The Alexander Silberman Institute of Life Sciences, The Hebrew University of Jerusalem, Edmond J. Safra Campus, Givat Ram, Jerusalem, Israel

[8]Department of Pathology, Wake Forest University School of Medicine, Winston-Salem, North Carolina, USA

Abstract

Despite the clear major contribution of hyperlipidemia to the prevalence of cardiovascular disease in the developed world, the direct effects of lipoproteins on endothelial cells have remained obscure and are under debate. Here we report a previously uncharacterized mechanism of vessel growth modulation by lipoprotein availability. Using a genetic screen for vascular defects in zebrafish, we initially identified a mutation, *stalactite* (*stl*), in the gene encoding microsomal triglyceride transfer protein (*mtp*), which is involved in the biosynthesis of apolipoprotein B (ApoB)-containing lipoproteins. By manipulating lipoprotein concentrations in zebrafish, we

Correspondence should be addressed to K.Y. (karina.yaniv@weizmann.ac.il).
[9]These authors contributed equally to this work.

Note: Supplementary information is available in the online version of the paper.

AUTHOR CONTRIBUTIONS

I.A.-D. conducted experiments, data analyses and wrote the manuscript. Y.E., V.N.P., M.G., G.M., L.G.-B. and O.M. performed zebrafish experiments. G.A. managed the fish facility. D.C., B.L., J.U., K.K. and K.S. contributed to the F3 mutagenesis screen. C.M.W. and T.T.C. performed *in vitro* studies. I.R. performed lipidomics analyses. W.W. and P.M.M. provided the *ApoE*-null mice. S.A.F. provided advice in lipids studies. L.C. conducted statistical analyses and developed software for quantification. G.S.S. supervised *in vitro* experiments and provided advice in lipids studies. M.L.I.-A. supervised *in vitro* studies. B.M.W. supervised the initial zebrafish studies and provided advice throughout the project. K.Y. conducted experiments and data analyses, wrote the manuscript and supervised the project.

COMPETING FINANCIAL INTERESTS

The authors declare no competing financial interests.

found that ApoB negatively regulates angiogenesis and that it is the ApoB protein particle, rather than lipid moieties within ApoB-containing lipoproteins, that is primarily responsible for this effect. Mechanistically, we identified downregulation of vascular endothelial growth factor receptor 1 (VEGFR1), which acts as a decoy receptor for VEGF, as a key mediator of the endothelial response to lipoproteins, and we observed VEGFR1 downregulation in hyperlipidemic mice. These findings may open new avenues for the treatment of lipoprotein-related vascular disorders.

We identified a zebrafish mutant, which we named *stalactite* (*stl*), with excessive sprouting angiogenesis, in a *Tg(fli1:eGFP)*^{y1} [1,2] transgenic-based forward genetic screen for vascular-specific mutations. *stl* mutants have ectopic angiogenic segments that extend ventrally from the subintestinal vessels (SIVs) (Fig. 1a, b), a vascular bed that initially forms bilaterally over the dorsal-lateral aspect of the large zebrafish yolk cell (Supplementary Fig. 1). A quantitative analysis (Supplementary Fig. 1) revealed both greater numbers and longer lengths of ventral SIV sprouts in *stl* mutants (Fig. 1c) compared to their wild-type (WT) siblings. At slightly later stages of development, we also found excessive angiogenic branching in the dorsal part of the intersegmental vessels (ISVs) in *stl* mutants compared to their WT siblings (Fig. 1d, e). We counted endothelial nuclei in the yolk areas of WT and *stl; Tg(fli1:neGFP)*^{y7} embryos to determine whether formation of ectopic sprouts in *stl* mutants involves overproliferation of endothelial cells. The total number of endothelial cells in the yolk area was 42% higher in *stl* mutants than in their WT siblings, with excess cells being found exclusively in the ectopic ventral sprouts of the mutant embryos (Fig. 1f, g). *stl* mutants also had defects in yolk absorption (Supplementary Fig. 1), and *stl* mutant larvae died by approximately 6 days post fertilization (dpf).

To examine the molecular nature of the *stl* phenotype, we positionally cloned the defective locus. We genetically mapped the mutation to an interval in linkage group 1 that contains the gene encoding microsomal triglyceride transfer protein (*mtp*). Sequence analysis of *mtp* complementary DNA (cDNA) from *stl* mutants and their wild-type siblings revealed a change in a conserved leucine residue (Leu475) to a proline in the mutants (Supplementary Fig. 2). MTP, an intraluminal protein found within the endoplasmic reticulum of the liver and intestine, is required for the assembly and secretion of proatherogenic, ApoB-containing lipoproteins such as chylomicrons, very-low-density lipoproteins and low-density lipoproteins (LDLs)[3]. After their assembly into mature particles, ApoB lipoproteins are secreted into the blood and lymph stream. Although the MTP-ApoB pathway was originally thought to be unique to the liver and intestine, the findings that the mouse yolk sac expresses Mtp and that mice homozygous for an *Mtp* gene disruption die at embryonic day 10.5 (ref. 4) underscores the key role of the synthesis and secretion of ApoB-containing lipoproteins during early embryogenesis. The yolk syncytial layer (YSL) of zebrafish (the functional counterpart of the yolk sac of higher vertebrates) expresses *mtp* starting at the gastrula stage[5] and forms ApoB-related lipoproteins, which enter the circulatory system and deliver nutrient lipids to the tissues [6–8]. As in mice and humans, zebrafish MTP is involved in lipoprotein assembly in the YSL and is also found at later stages of development in the intestine and liver [5,9]. In addition, zebrafish have structural and functional homologs of mammalian ApoAI, ApoCII, ApoE, phospholipase A2 (PLA2) and lipoprotein lipase (LPL)[10,11].

Four additional lines of evidence confirm that a mutation in *mtp* is responsible for the *stl* phenotype. First, injection of antisense morpholino oligonucleotides targeting *mtp*[6] reproducibly phenocopied the angiogenesis and yolk absorption phenotypes seen in *stl* mutants (Supplementary Fig. 3a, b, d). Second, injection of *mtp* mRNA into *stl* mutants suppressed ectopic sprouting, and mRNA-rescued larvae survived for at least 10 dpf (Supplementary Fig. 3a, c, e). Third, downregulation of *apoB* using *apoB* morpholino

oligonucleotides led to ectopic SIV branching that was reminiscent of that seen in the *stl* mutants (Supplementary Fig. 3f). However, we did not observe this proangiogenic response upon downregulation of *apoA1* (Supplementary Fig. 3g). Finally, reduction of LDL concentrations in WT embryos using atorvastatin[12] efficiently phenocopied the phenotype of excess angiogenesis seen in *stl* mutants (Fig. 1h, i). Together, these results confirm the specificity of the MTP-ApoB pathway in causing excess angiogenesis.

The restricted expression of the *mtp* transcript in the yolk syncytium, liver and intestine[5] and the lack of vascular *mtp* expression (Supplementary Fig. 3h) strongly suggest that the role of this gene in vessel development is not cell autonomous. To confirm this notion, we injected *mtp* mRNA into the yolk syncytium of WT and *stl* mutant zebrafish at the dome stage. As the cytoplasmic bridges between the embryo and the yolk cell are closed already by the 1,000-cell stage[13] (before the dome stage), reagents injected into the yolk cell after this stage are restricted exclusively to the yolk syncytium. As expected for a YSL-specific defect, injection of *mtp* mRNA at the dome stage yielded efficient rescue of the excessive angiogenesis phenotype in *stl* mutants (Supplementary Fig. 3e).

In humans, mutations in *MTP* are the proximate cause of abetalipoproteinemia[14–16], an autosomal-recessive defect in the production of ApoB-containing lipoproteins that results in a virtual absence of LDL in the blood. To confirm that the effects of *mtp* downregulation on lipoprotein production and secretion are conserved in zebrafish, we stained WT and *stl* mutant zebrafish larvae with Oil Red O (ORO)[6]. *stl* mutants had a clear absence of lipids in their vasculature when compared to their WT siblings (Fig. 1j). To further confirm the lipoprotein-depletion phenotype, we performed a detailed lipid profile analysis of the *stl* mutants. Taking advantage of the fact that exogenously supplied, radioactively labeled fatty acids are properly processed by zebrafish larvae and are found as expected in the triglyceride fraction[17], we used thin-layer chromatography to confirm that the concentrations of triglycerides are strongly reduced in *stl* mutants (Supplementary Fig. 4). We also found reduced concentrations of cholesterol using gas chromatography–mass spectrometry (GC-MS) (Supplementary Fig. 4).

To further characterize the effects of lipoproteins on angiogenesis *in vivo*, we generated a zebrafish model of lipoprotein overload in the circulation by downregulating the *apoCII* gene[18,19]. ApoCII is a component of ApoB-containing lipoproteins and is required for the activation of the enzyme LPL in capillaries. LPL activation leads to triglyceride hydrolysis and the release of free fatty acids for use by cells (reviewed in ref. 20). In humans, mutations in *APOCII* result in the accumulation of unprocessed lipoproteins in the circulation (hyperlipoproteinemia type IB and hypertriglyceridemia) and in increased risk of early atherosclerosis[21–23]. We reasoned that whereas morpholino knockdown of *apoCII* early in development would lead to a global reduction in lipid delivery, the endothelial cells of these morphants would nevertheless be exposed to elevated concentrations of plasma lipoproteins, mimicking the hyperlipidemia seen in *APOCII* mutant humans. Injection of *apoCII* morpholino oligonucleotides into *Tg(fli1:eGFP)*^{y1} embryos resulted in increased intravascular concentrations of lipoproteins, as assessed by ORO staining at 4 dpf (Fig. 2a; compare with Fig. 1j). This increase was accompanied by a marked reduction in total triglyceride and cholesterol levels (Supplementary Fig. 4). In contrast to the excess angiogenesis phenotype seen in *stl* mutants, however, we found no ectopic SIV sprouts in *apoCII* (Fig. 2b, c) or *lpl* morphants (Supplementary Fig. 4), confirming that global lipoprotein starvation *per se* does not lead to excessive angiogenesis. On the contrary, high lipoprotein concentrations in the circulation of *apoCII* morphants resulted in a poorly developed vasculature that was characterized by short and partially lumenized ISVs (Fig. 2d–f). These results are consistent with previous findings describing premature vascular

disease[24] and general endothelial dysfunction[25] under hyperlipoproteinemic conditions in humans[26].

To further show that the angiogenic phenotypes seen in *stl* and *apoCII* morphants result from a direct response of endothelial cells to lipoprotein concentrations and not from alternative cues trigged by fatty-acid depletion, we investigated the ability of exogenously supplied fatty acids to restore a normal vasculature. The addition of short-, intermediate- or long-chain fatty acids to the embryo culture media did not rescue the vascular phenotype of *stl* mutants (Fig. 2g, h) or *apoCII* morphants (Fig. 2i, j and data not shown), even when applied at high concentrations (Supplementary Fig. 4), consistent with the notion that the angiogenic phenotypes result from a direct response of the endothelial cells to lipoprotein concentrations.

To elucidate the mechanisms underlying the effects of lipoproteins on vascular growth, we began by searching for endothelial-specific mRNAs whose expression was affected by changes in lipoprotein concentrations. Quantitative real time PCR (Fig. 3a) and *in situ* hybridization (Supplementary Fig. 5) revealed that the *vegfr1* mRNA levels were lower in *mtp* morpholino oligonucleotide-injected embryos than in uninjected siblings at 24 h post fertilization (hpf). This reduction was specific for *vegfr1,* as we found little change in the levels of *vegfr2* or *vegfr3* mRNAs or in the mRNA levels of other vascular genes in the *mtp* morphants (Fig. 3a and Supplementary Fig. 5). VEGFR1 protein concentrations were also strongly downregulated in *stl* mutants but were substantially upregulated in *apoCII* morphants, in which endothelial cells face high concentrations of ApoB lipoproteins (Fig. 3b). We found similar effects on VEGFR1 levels in endothelial cells *in vitro*. Treatment of cultured human umbilical vein endothelial cells (HUVECs) with LDL elicited an increase in VEGFR1 but not VEGFR2 concentrations (Fig. 3b). In addition, hyperlipidemic *Apoe*- or *Ldlr*-null mice (reviewed in refs. 27,28) also showed increased endothelial-specific Vegfr1 expression compared to control WT mice (Fig. 3c–e), confirming conservation of this pathway in higher vertebrates.

Previous studies have shown that VEGFR1 has an inhibitory role in angiogenesis, acting as a ‘sink’ for the VEGF ligand[29–31]. Downregulation of *vegfr1* by an ATG-blocking morpholino oligonucleotide resulted in excessive sprouting and branching from the SIV plexus and trunk ISVs, resembling the phenotype of *stl* mutants (Supplementary Fig. 5). We reasoned that if lipoprotein depletion promotes angiogenesis by downregulation of VEGFR1, we should be able to rescue the proangiogenic phenotype of the *stl* mutants by restoring VEGFR1 expression. Indeed, injection of *vegfr1* mRNA into *stl* mutant embryos suppressed ectopic SIV sprouting (Fig. 3f, g). Furthermore, siRNA-mediated downregulation of *VEGFR1* (Fig. 3h) abolished the ability of cultured HUVECs to respond to LDL levels in both wound-healing and Boyden-chamber (data not shown) assays.

The changes in *vegfr1* mRNA levels observed in *stl* mutants (Fig. 3a) and *Apoe*-null mice (Fig. 3e) could have resulted from either transcriptional regulation or post-transcriptional modifications altering the stability of the *vegfr1* transcript. To distinguish between these two possibilities, we took advantage of a transgenic zebrafish line that expresses yellow fluorescent protein (YFP) under the regulation of the *vegfr1* promoter[32]. In these animals, YFP expression recapitulates the pattern of endogenous *vegfr1* expression[32]. However, the YFP cassette possesses its own 3′ untranslated region (Online Methods); hence, YFP expression would not be subject to post-trasncriptional modifications mediated by the 3′ untranslated region of the *vegfr1* gene. We hypothesized that if APOB-lipoproteins regulate *vegfr1* mRNA expression at the transcriptional level, downregulation of *mtp* will result in a significant decrease in the levels of *yfp* mRNA. If in turn, *vegfr1* downregulation involves alterations in its mRNA stability, the levels of *yfp* mRNA will remain unchanged upon *mtp*

morpholino oligonucleotide injection. *mtp* knockdown resulted in a significant (P=0.0248) decrease in YFP expression (Fig. 3i, j), providing evidence that ApoB-containing lipoproteins inhibit *vegfr1* expression at the transcriptional level. Whether this regulation is direct or indirect remains to be determined.

Because the vascular phenotype of *stl* mutants was not trigged by global lipid starvation (Fig. 2), we hypothesized that lowered concentrations of lipoproteins in mutant animals, directly sensed by endothelial cells, exert a proangiogenic response. To test this hypothesis, we first examined whether exogenously supplied LDL could suppress ectopic sprouting in *stl* mutants when applied intravascularly. Injection of LDL labeled with the lipophilic carbocyanine DiI into 2.5-dpf *stl* mutants resulted in a strong reduction in both the number and length of the ectopic SIV sprouts (Fig. 4a, b), suggesting that circulating lipoproteins can activate antiangiogenic mechanisms in endothelial cells.

To further confirm the cell-autonomous nature of the endothelial response, we designed an *in vivo* approach to allow for the localized delivery of exogenous ApoB particles in the proximity of angiogenic vessels. Lipoprotein-secreting HEK293 cells cotransfected with vectors encoding the human forms of MTP and ApoB34 (ref. 33) (Supplementary Fig. 6a) or untransfected HEK293 control cells were transplanted into the perivitelline space on one side of 2.5-dpf *stl; Tg(fli1:eGFP)*^{y1} embryos in close proximity to the forming SIVs (Fig. 4c). ApoB34 is a truncated form of ApoB that was shown to be properly assembled and secreted in the presence of MTP[33]. We chose to use this construct as it is the shorter form of ApoB whose secretion is MTP dependent. Lipoprotein-secreting cells impeded the migration of endothelial cells and the growth of ectopic sprouts in the area of transplantation (Fig. 4d). Ectopic SIV sprouting, however, was not affected on the untransplanted side of the same embryos (Fig. 4d), confirming that the localized transplantation did not result in systemic rescue of the *stl* phenotype. Non–lipoprotein-secreting cells, in contrast, did not impede endothelial migration or sprouting (Fig. 4d). Quantitative analysis revealed a much lower amount of endothelial migration onto lipoprotein-producing when compared to non–lipoprotein-producing cells (Fig. 4e and Supplementary Fig. 6b). We also found a similar direct inhibitory effect of LDL on the migration of HUVECs and human aortic endothelial cells (HAECs) *in vitro* using either Boyden-chamber (Supplementary Fig. 7a) or wound-healing (Supplementary Fig. 7b) assays. We observed these effects even at concentrations of LDL that did not affect cell proliferation (Supplementary Fig. 7c). It is notable, however, that LDL concentrations that are considered pathological in humans (>160 mg dl^{-1}) result in endothelial cell death *in vitro* (ref. 34 and data not shown). Taken together, these results indicate that endothelial cells respond in a cell-autonomous manner to changes in ApoB-containing lipoprotein concentrations. Although it is unclear whether this response involves the interaction of lipoproteins with the luminal or abluminal surface of endothelial cells, direct contact between the lipoprotein and endothelial cells seems to be needed, as lipoprotein-secreting cells that were not placed in close proximity to developing vessels did not induce inhibitory effects (data not shown). Further studies will be required to ascertain whether there are luminal and abluminal receptors within endothelial cells for lipoprotein present in different areas of the vessel microenvironment.

We next asked which component of ApoB-containing lipoproteins elicits an endothelial response. Taking advantage of the fact that *stl* mutants lack secreted ApoB-containing lipoproteins, we attempted to rescue the vascular phenotype of the mutants by restoring lipid or protein components individually (Fig. 4f–i). Although an intravascular supply of free fatty acids did not rescue the ectopic branching phenotype of the mutants, injection of a delipidated form of ApoB-100 (Online Methods) substantially reduced the number and length of the ectopic angiogenic sprouts (Fig. 4f–i). Apo B-100 is the full-length form of the endogenous *apoB* gene, encoding a 550-kDa protein, which is essential for the assembly and

secretion of ApoB-containing lipoproteins from the liver (very–low-density lipoprotein, LDL and intermediate-density lipoprotein). These results strongly support the idea that the ApoB protein itself, but not the lipid moieties within the lipoprotein, acts on endothelial cells to regulate angiogenesis.

Endothelial-lipoprotein interactions have direct relevance to atherogenesis, thrombosis and other cardiovascular diseases. The results presented here reveal an intrinsic capacity of ApoB-containing lipoproteins to control vascular growth by regulating the expression of VEGFR1 in endothelial cells (Fig. 4j).

Previous data has hinted at direct interactions between LDL and VEGF receptors *in vitro*[35,36], but the molecular mechanisms regulating this interplay have remained unclear. Here we show that expression of VEGFR1 is regulated *in vivo* by the availability of ApoB-containing lipoproteins. Moreover, we show that this regulation is achieved primarily at the transcriptional level. However, the molecular pathways responsible for this regulation are unknown, including which receptors within the endothelial cells mediate the uptake of lipoproteins or provide signals in response to lipoprotein particle abundance. The finding that endothelial cells of *Ldlr*-null mice express elevated amounts of Vegfr1 highlights the potential role of alternative lipoprotein receptors in mediating the endothelial response.

Recent evidence suggests a potentially crucial role for the nutritional state of tissues in vessel growth[37–39]. By taking advantage of our new zebrafish models of hypolipidemia and hyperlipidemia, we show that the effects of ApoB-containing lipoproteins on angiogenesis are not trigged by a reduced delivery of fatty acids to tissues or to global lipid starvation, as *apoCII* deficiency in zebrafish embryos did not phenocopy the vascular phenotype that resulted from the loss of MTP. Furthermore, the high plasma concentrations of triglyceride-rich ApoB-containing lipoproteins in these animals inhibited angiogenesis, as did exogenous delivery of LDL. This effect, however, required the presence of ApoB as intravascular delivery of a delipidated form of ApoB-100, but not of free fatty acids, efficiently reverted the excessive angiogenesis phenotype of *stl* mutants. Although we cannot exclude the possibility that the fate of delipidated ApoB in circulation might involve its association with endogenous plasma lipid moieties, our results support the notion that ApoB itself provides the crucial signal for the antiangiogenic effects.

Several pathological conditions involve dramatic alterations in lipoprotein concentrations, resulting in a wide variety of vascular-related diseases. Our results have uncovered a new mechanism for the regulation of developmental angiogenesis by ApoB-containing lipoproteins that seems to be reactivated during pathological conditions of hyperlipidemia. These findings may provide an explanation for the endothelial dysfunction that precedes the formation of atherogenic plaques, as well as for the impaired collateral vessel growth that is observed in patients with hypercholesterolemia. Furthermore, these findings raise key questions about the potential effects of circulating lipoproteins during tumor-related angiogenesis.

ONLINE METHODS

Zebrafish husbandry and transgenic lines

Zebrafish were raised by standard methods[40] and were handled according to the guidelines of the Weizmann Institute Animal Care and Use Committee. The *Tg*(*fli1:eGFP*)^{y1} and *Tg*(*fli1:neGFP*)^{y7} (Ref. 1,2) lines were previously generated. The *Tg*(*flt1:YFP*)^{hu4624}(Ref. 32) line was generated by inserting a cassette of *yfp* with its own 3′ untranslated region (the simian virus 40 (SV40) late poly(A) region from the plasmid pCS2^{+}) and the *neo* gene conferring neomycin resistance at the translational start of the *vegfr1* gene.

Positional cloning

Generation of the lines used for genetic mapping of the *stl* mutation, the bulk segregant analyses, the genomic DNA isolation and PCR were performed as described elsewhere [41]. Oligonucleotide sequences for Z7573 (5′-TGTTGCACCATATTGTGGCT-3′ and 5′-AGACAAGAAAGGGGTCTGCA-3′), Z26148 (5′-CAACTTTGCGAGTGCTTTCA-3′ and 5′-TGGAGTGGTGTGTGTTGCTT-3′) and Z49706 (5′-TTCGGTATGCACAAATACGC-3′ and 5′-GTGCAGTTTGCGTCACTTGT-3′) were obtained at http://danio.mgh.harvard.edu/markers/ssr.html (ZV7) and http://www.ensembl.org/Danio_rerio/Info/Index (ZV7). Candidate SSR marker primer pairs 9273 (5′-CTTGGATGGCCTTGGGGAGAGT-3′ and 5′-GGGTGGTTGGGTGTTGTTGTTC-3′), 9606 (5′-GAGCCCACCACACCATCAG-3′ and 5′-AAAGCCATTCACATTCATAGTAGG-3′) and 9522 (5′-AGGAGGAGTCTGAGGTTC-3′ and 5′-GTAGATGCGCTGGTTTTGATGGTA-3′) were generated using the Zebrafish SSR search website, Massachusetts General Hospital, Charlestown MA at http://danio.mgh.harvard.edu/markers/ssr.html

The primers used for PCR to identify SNPs for positional cloning were designed on the basis of the available zebrafish genomic sequence at http://www.ensembl.org/Danio_rerio/Info/Index, http://vega.sanger.ac.uk/index.html and http://www.sanger.ac.uk/Projects/D_rerio/WebFPC/zebra/small.shtml. Polymorphism analyses and sequence comparisons were performed using SeqMan alignment software (DNASTAR).

Generation of the pCS2*mtp*CDS and pCS2*vegfr1*CDS plasmids

We used the following primers to amplify the full-length coding sequences of zebrafish *mtp* and *vegfr1: mtp*: 5′-ATGATGCCGGTTGCCGGACT-3′ and 5′-TTACCAGGCCGGCTCAAAGA-3′; and *vegfr1*: 5′-GACCAAGAGAATGTTCGATATATTATTTGTG 3′ and 5′-TTAGAAACTGGGGTAAAGAAGATCGCCTTC-3′. After TOPO (Invitrogen) cloning and sequencing, a Gateway-compatible (Invitrogen) middle entry clone was generated using Gateway BP clonase (Invitrogen) mediated recombination. The *mtp* and *vegfr1* coding sequences were then transferred into a pCSDest vector using Gateway LR clonase (Invitrogen) mediated reaction to produce the pCS*mtp*CDS and pCS*vegfr1*CDS plasmids. After linearization with *NotI*, the plasmids were used as templates for mRNA synthesis.

Injection of zebrafish embryos

mtp[6], *apoCII* [18], *vegfr1* 5′-ATATCGAACATTCTCTTGGTCTTGC-3′, *apoB* 5′-CAACTTAGTGTCCATTTTTATCGGC-3′ and *apoA1* 5′-TCAGTGCAAGAGCCACGAATTTCAT-3′ morpholino oligonucleotides (Gene Tools) were resuspended and injected as described [1] at concentrations of 5–20 ng per embryo. We injected pCS2*vegfr1*CDS mRNA (1,200 ng per embryo) and pCS2*mtp*CDS mRNA (232 ng per embryo) at the one-cell stage and the dome stage, respectively.

Microangiography and cell transplants

Microangiography was performed at 2.5 dpf, as described[42]. Intravascularly injected solutions were as follows: 1 μg μl^{-1} DiI-LDL (Invitrogen), 10 μM atorvastatin (Sigma) in DMSO, 6 μg ml^{-1} hexanoic acid (C_6) and 0.5 μg μl–1 human ApoB-100 (Meridian Life Science, A50220H) in PBS supplemented with 0.5% fatty-acid–free BSA (Sigma, A8806). Human ApoB-100 is an artificially delipidated form of ApoB in which sodium deoxycholate is used to provide a stable environment for the ApoB protein to keep it in solution once the natural lipids are removed and to prevent its aggregation. The ApoB protein was solubilized in 0.5% fatty-acid–free BSA (Sigma, A8806), which renders it soluble in water[43]. HEK293

cells cotransfected with the plasmid Huh7MTP (encoding human MTP) and a plasmid encoding human ApoB34 (see below) or untransfected control cells were transplanted into the perivitelline space of one side of the yolk of 2.5 dpf *stl; Tg(fli1:eGFP)*^{y1} mutant or WT embryos ventral to the developing SIVs[44].

Microscopy and imaging

Zebrafish embryos used for imaging or *in situ* hybridization were treated with 0.003% phenylthiourea beginning at 8 hpf to inhibit melanin pigment formation. Confocal imaging was performed using a FV1000 Olympus imaging system or a Zeiss LSM780 upright confocal microscope equipped with X20 NA 1.0 lens, as described[1].

Fatty-acid feeding of zebrafish embryos

We incubated dechorionized 24-hpf embryos with 6 μg ml^{-1} short-(hexanoic acid, Sigma, 12137), intermediate-(dodecanoic acid, Sigma, L4250) or long-chain fatty acid (oleic acid, Sigma, 01383) in embryo medium supplemented with 0.1% fatty-acid–free BSA (Sigma, A8806) for 48 h. Embryos were then fixed overnight in 4% paraformaldehyde and processed for alkaline phosphatase staining[45].

Lipid content measurements

Triglyceride content measurements—We incubated dechorionized 24-hpf embryos with 2 μCi ml^{-1} [^{3}H]-oleic acid (Perkin Elmer NET289005MC) in a fatty-acid–free solution (Sigma, A8806) containing 0.1% BSA and 3 μg ml^{-1} oleic acid (Sigma, O1383) for 48 h. After deyolking, we homogenized the embryos in 1 ml cold methanol and extracted the lipids following the method of Bligh and Dyer [46] by adding ice-cold chloroform and double distilled water. We collected the lower chloroform phase, evaporated it under vacuum or N_2 and kept it at −20 °C. We developed the lipids on silica gel 60 thin-layer chromatography plates in a solvent system of petroleum ether, diethyl ether and acetic acid (80:20:1). Labeled lipids were visualized with autoradiography, and spots corresponding to the triglyceride standards (Sigma 17811) were scraped and quantified using liquid scintillation fluid.

Cholesterol content measurements—For GC-MS, samples were lyophilized for 2 h, and 10 μl of pyridine and 80 μl of N-methyl-N-(trimethylsilyl)trifluoroacetamide were added to the dry residue. The samples were then shaken vigorously for 30 s, and the mixture was transferred to a 2-ml autosampler glass vial with a 100-ml conical glass insert. After capping the vial, the reaction mixture was incubated at room temperature for at least 1 h. The GC-MS instrument and analytical parameters used were as described by Itkin *et al*[47]. with some modification: the CT-split 1:25 mode was used here. Xcalibur software version 1.4 (Thermo Finnigan) was used for data analysis. Cholesterol present in the samples was identified as O-Trimethylsilylcholesterol by a comparison of its retention time and mass spectrum for the sample mixture to those generated for the cholesterol authentic standard silylated as mentioned above, and analyzed using the same analytical parameters on the same instrument. The samples were injected in randomized order; the mix of alkanes, injected after each several biological samples, was utilized as quality control. The reconstructed ion chromatogram generated from the characteristic fragments of silylated cholesterol (329, 353, 368 and 458 Da) was used for the calculation of peak areas.

In situ hybridization and ORO and alkaline phosphatase staining

Embryos were fixed overnight in 4% paraformaldehyde and processed for alkaline phosphatase staining[45], ORO staining[6] or whole-mount *in situ* hybridization using antisense mRNA probes for *vegfr1*, *vegfr2, vegfr3* and *cdh5*, as described[48].

Zebrafish western blot

Three-dpf zebrafish embryos were processed for western blot, as described[1]. VEGFR1 was detected using a 1:500 dilution of a custom made chick polyclonal serum (Aves Labs) generated against the peptide CZ TKD TDT KGR FSS PVL DVT EKQ. Blots were then reblocked by standard protocols and probed with a 1:5,000 dilution of antibody to tubulin (Sigma, T3526).

Fluorescence-activated cell sorting (FACS) of endothelial cells from zebrafish embryos

We used 3-dpf *Tg*(*fli1:eGFP*)^{y1} embryos for FACS of GFP-labeled endothelial cells. Single-cell suspensions were prepared as described in Takada *et al.*[49]. Sorting was performed at 4 °C in a FACSAria cell sorter using a 70-μm nozzle. GFP$^+$ and GFP$^-$ cells were separately collected in 1 ml FCS. Sorted cells were washed with PBS and centrifuged at 300 *g* at 4 °C for 5 min twice. The cell pellet was suspended in 1 ml TRIzol for RNA extraction.

Total RNA isolation from zebrafish embryos, semiquantitative and quantitive real-time PCR analyses

We homogenized 30–60 WT or *mtp* morpholino-oligonucleotide–injected embryos in TRIzol (Invitrogen) and processed them for RNA extraction following standard procedures. After precipitation, we treated the RNA with DNase using the DNA free kit (Ambion) to eliminate genomic DNA. One microgram of total RNA per reaction was reverse transcribed using the ThermoScript RT-PCR kit (Invitrogen). In the *yfp* measurement experiments, an RNeasy mini kit (QIAGENE) was used for RNA extraction, and 1 μg of total RNA per reaction was reverse transcribed using a High Capacity cDNA Reverse Transcription Kit (Applied Biosystem).

To measure relative changes in mRNA transcripts we used the following primers: *vegfr1*: 5′-TGGTCATATGGAGTCCTGCTC-3′ and 5′-CATGTTGAGTCCTGGGTATGG-3′; *vegfr2:* 5′-CTGGTGGAGAGGCTAGGAGA-3′ and 5′-TGATCGGGATGTAGTGCTTTC-3′; *vegfr3*: 5′-TAACCAACCCCTCCATCAGA-3′ and 5′-CTGAATGCTGAGAGTCCGATT-3′; *cdh5: 5′*-GCACATGAAGATGTGTTGAATG-3′ and 5′-TGGTTAGTTCTGGTGCATTGTC-3′; *fli1*: 5′-CCATCTCACGGCTGACCAGT-3′ and 5′-GACAGCGCACACAACCAC-3′; and *yfp*: 5′-CACATGAAGCAGCACGACTT-3′ and 5′-GGTCTTGTAGTTGCCGTCGT-3′ (ref.[50]). Expression levels were standardized to the primer set specific for *ef1a* and *b-actin: ef1a*: 5′-CCTCTTTCTGTTACCTGGCAAA-3′ and 5′-CTTTTCCTTTCCCATGATTGA-3′; and *b-actin*: 5′-TGACAGGATGCAGAAGGAGA-3′ and 5′-GCCTCCGATCCAGACAGAGT-3′ (ref.[50]). Reactions were run in 96-well plates in a LightCycler 480 Real-Time PCR System (Roche) or in a Step One Plus real time PCR system (Applied Biosystems), and the results were analyzed using built-in software. Measurements were conducted in duplicate.

For semiquantitative real-time PCR, we used the following primers to measure relative changes in *mtp* mRNA transcripts: 5′-CCGTCTTACATGGAGGTGAA-3′ and 5′-CGGACATGGAGAACATCTTG-3′. Expression levels were standardized to the primer set specific for *b-actin*: 5′-CAGCTAGTGCGAATATCATCT-3′ and 5′-TTTCTGTCCCATACCAACC-3′.

Cell cultures and reagents

We cultured HAECs (VEC Technologies) and HUVECs (VEC Technologies and Promo Cells) in complete MCDB 131 medium (VEC Technologies) or in M199 medium supplemented with ECGS (Zotal).

Immunoblotting and immunoprecipitation

HUVECs were lysed for 30 min in lysis buffer (50mM Tris, pH7.4, 150mM NaCl, 1% NP40, 0.25% sodium deoxycolate, 1mM EDTA, 1mM sodium vanadate, 10mM beta-glycerophosphate and proteinase inhibitors (1mM phenylmethanesuldonylfluoride (PMSF), 20μg/ml leupeptin and 20μg/ml aprotinin) buffer. Proteins were separated by SDS-PAGE and transferred to nylon membranes (Whatman). Membranes were then probed with antibodies to VEGFR2 (Cell Signaling, 2479, 1:1,000), VEGFR1 (R&D, AF471, 1:500) or tubulin (Abcam, ab15246, 1:1,000) and detected by enhanced chemiluminescence (Thermo Fisher Scientific).

Boyden-chamber assays

HUVECs or HAECs (50,000 per well) were seeded on the top well of a Boyden chamber (5-μm pore size) and cultured overnight at 37 °C and 5% CO_2. Subsequently, the bottom wells were filled with either LDL^- serum or LDL^- serum supplemented with 10 μg ml^{-1} LDL (Sigma, L7914) for overnight incubation. After incubation was completed, we scraped off the endothelial cells that remained on the upper side of the membrane using a cotton swab. Endothelial cells that had transmigrated were stained with DAPI and imaged using fluorescent microscopy. We counted positive nuclei in three random image fields. We conducted three individual experiments and used the averages to generate the bar graph.

Generation of LDL^- serum

We generated LDL^- serum by purification of complete media using Seppro IgY14 spin columns (Sigma, SEP010).

Wound-healing assay

We plated HUVECs (either exposed to the indicated siRNAs or not) to confluency for the wound-healing assays. A 200-μm wound was inflicted with a 10-μl pipet tip and was treated with either 1% LDL^- serum, 1% LDL^- serum supplemented with 10 μg ml^{-1} LDL or vehicle. Cells were imaged by time-lapse video microscopy for 24 h. To calculate the cell migration rate, the wound area was determined prior to and after completion of the experiment (8 h between measurements). We measured four wells per experimental group in four independent experiments. Results were normalized to control (identical media in the absence of LDL) and expressed as migration area over control.

siRNA experiments

We obtained the siRNA reagents from Dharmacon Research (Chicago, Illinois). Endothelial cells in 90% confluency were transfected with DharmaFECT transfection reagents in the absence of antibiotics. For transfection, either *VEGFR1* siRNA SMARTpool or nontargeting siRNA (siCONTROL) was used at 100 nmol l^{-1} following the manufacturer's instructions. Efficiency of the siRNA was evaluated by standard western blots against VEGFR1 and resulted in a 78–85% reduction in the total levels of VEGFR1 protein. Experiments on migration were conducted 48 h after transfection.

MTT cell proliferation assay

We plated HUVECs in 96-well plates (coated with 0.2% gelatin) at a density of 2,000 cells per well in 0.2 ml M199 growth medium. After 24 h, the cells were washed and were incubated with either 20% lipoprotein-depleted serum (LPDS) or 20% LPDS supplemented with 10 or 25 μg ml^{-1} LDL for the indicated periods. The number of cells was then determined using an MTT cell growth assay according to the protocol of Hansen *et al.*[51]. Briefly, MTT reagent (Sigma, M5655) was added to the wells at a final concentration of 0.6

mg ml^{-1}, and the cells were further incubated at 37 °C for 2 h. The reaction was terminated by adding 100 μl per well of an extraction solution consisting of 20% SDS in a 50% dimethylformamide (DMF) solution. Absorbance was read at 570 nm using an ELISA plate reader after leaving the plates protected from light overnight.

Preparation of LPDS

We added 200 gr of solid KBr (Sigma, P-5912) to 500 ml of FCS (Gibco, 10270-106) and stirred it until completely dissolved. We then centrifuged the serum at 40,000 rpm for 48 h at 4°C. After centrifugation, we collected the upper 20–25% of the volume using a syringe and needle. We then dialyzed the serum against 5 liter of 150 mM NaCl, 2mM Tris-Cl (pH 7.4), 0.01% NaEDTA and changed the buffer five to six times over a period of ~10–16 h (total dialysis volume 25–30 liters). We adjusted the volume back to 500 ml with the dialysis buffer, heat inactivated the serum (56°C, 30 min) and sterilized it by filtration through a 0.22-mm cellulose acetate membrane. Aliquots are kept frozen at −20°C until used.

Cloning of human *MTP*

We amplified human *MTP* cDNA by RT-PCR using Huh7 (human hepatoma) cell RNA and the primers 5′-AGAAAGCTTGCTGGTCAATATGATTCTTCTTGC-3′ and 3′-AGATCTAGAATCACAGGTCAGTTTCAAAACCATCC-5. After digestion of the primer-encoded restriction enzyme sites with HindIII and XbaI, the PCR product was ligated into the HindIII and XbaI sites of the plasmid pCMV5. The resulting plasmid insert was sequenced and found to encode an identical 894 amino acid sequence as GenBank locus EAX06106.1 (microsomal triglyceride transfer protein (*Homo sapiens*)). The resulting plasmid was named Huh7MTP.

HEK293 cell transfection

HEK293 cells at 50% confluency were cotransfected with 1 μg each of a plasmid expressing C-terminal FLAG-tagged apoB34 (apoB34F)[52] and Huh7MTP for 6 h using FuGENE 6 (Roche). After the transfection, the cells were labeled with CellTracker Orange CMRA (Invitrogen) for 45 min and grown overnight in serum supplemented DMEM.

Analysis of ApoB secretion from COS7 cells

We transfected apoB34F into HEK293 cells without (−) or with (+) the Huh7MTP plasmid. Twenty-four hours after transfection, cells were radiolabeled with ^{35}[S]methionine and ^{35}[S]cysteine for 3 h, and the cell lysate and culture medium were subjected to immunoprecipitation with 5 μg of affinity-purified ApoB-specific antibody (Academy Biomedical Co., Houston, TX, 20A-G1) followed by 8% SDS-PAGE and PhosphorImager analysis.

Quantitative analysis of HEK293 cell transplants

WT and *stl; Tg(fli1:eGFP)*^{y1} mutant embryos at 3.5 dpf that had been successfully transplanted with fluorescently labeled HEK293 cells adjacent to green fluorescent endothelial cells, were imaged. The total length of the interface between the endothelial and transplanted cells (Supplementary Fig. 6, blue = L1), as well as the total length of overlap between the two cell populations (Supplementary Fig. 6, yellow = L2), was traced and measured. The ratio $r = L2/(L1 + L2)$ was used to measure the ability of endothelial cells to migrate over the ApoB-secreting cells.

Mice and immunofluorescence

Apoe- and *Ldlr*-null mice (Jackson Laboratory) in the C57BL/6 background and the corresponding WT C57BL/6 controls (Jackson Laboratory) were handled according to the Weizmann Institute Animal Care and Use Committee. All analyses were performed using mice at 8–38 weeks of age fed with a normal chow diet. After anesthesia, the aortas of the mice were dissected and frozen for further PCR analyses or fixed for 3 h in 4% paraformaldehyde, equilibrated for 36 h in 30% sucrose in PBS-Tween, embedded in Tissue-Tek O.C.T. Compound (4583) and frozen at −80 °C. Slides of 7-μm sections were fixed in cold methanol, blocked with BSA and goat serum and stained overnight with antibody to CD31 (BD, 550274, 1:100) and antibody to VEGFR1 (Abcam, AB2350, 1:100). Slides were then incubated for 2 h with Cy3 anti-rabbit (Jackson, 111-485-045, 1:100) and Cy2 anti-rat antibodies (Jackson, 112-505-003, 1:100), stained with DAPI (10 mM Inno-Train Diagnostik) and mounted in fluorescent mounting medium. Images were captured using a Zeiss LSM780 confocal microscope.

RNA isolation from mouse aortic tissue and RT-PCR analyses

We homogenized dissected aortas from C57BL/6 and *Apoe*-null mice (500 mg of tissue per sample) in TRIzol and processed them for RNA isolation and semiquantitative PCR, as described[53]. For all samples, cDNA was generated from equal amounts of RNA (600 ng).

To measure the relative changes in *Vegfr1* mRNA transcripts, we used the following primers: 5′-GGCCCGGGATATTTATAAGAAC-3′ and 5′-CCATCCATTTTAGGGGAAGTC-3′. Expression levels were standardized to the primer set specific for *b2-microglobulin*: 5′-GTCTCGATCCCAGTAGACGG-3′ and 5′-TGGTGCTTGTCTCACTGACC-3′. Quantitative analyses were performed using ImageJ.

Statistical analyses

Error bars of mean data points are ± s.e.m. Comparisons of two populations were done with unpaired two-tailed *t* test assuming unequal variance of the populations (Figs. 1,3 and 4). Comparison of multiple populations was done using one-way analysis of the variance (ANOVA) (Fig. 2). Testing whether two populations are drawn from identical distributions was done using the χ^2 test (Fig. 2). To compute significance for the difference between two values, each representing a mean of a population, we tested the deviation of the ratio between them from 1 using a two-tailed *z* test (Fig. 3). All statistical tests were performed in Matlab. We used the *ttest2* function for *t* test, and the *anova1* function for ANOVA. We relied on the function normcdf to perform the *z* test, and on the function chi2cdf to perform the χ^2 test.

Supplementary Material

Refer to Web version on PubMed Central for supplementary material.

Acknowledgments

The authors would like to thank G. Palardy, R. Miyares, N. Nevo, I. Harel, T. Berkutzki, I. Raviv, R. Oren and C. Rot for technical assistance; A. Aharoni for help with GC-MS analyses; E. Zelzer (Weizmann Institute, Israel) for providing the *Ldlr*-null mice, K. Tordjman (Sourasky Medical Center, Israel) for providing the *ApoE*-null mice, S. Schulte-Merker (Hubrecht Institute) for providing the *vegfr1* plasmid and the *Tg*(*flt1:YFP*)^{hu4624} transgenic line; J. Berliner (University of California Los Angeles, California) for providing human aortic endothelial cells (HAECs); D. Haratz, I. Groskop and A. Shaish for advice regarding lipid analyses; A. Harmelin and N. Stettner for animal care; and I.B. Dawid, E. Tzahor, A. Gross, B. Shilo and J. Torres-Vazquez for critical reading of the manuscript. The authors are grateful to all the members of the Yaniv and Weinstein labs for discussion, technical assistance and continuous support. This work was supported in part by Israel Science Foundation 748/2009 (to K.Y.), Marie Curie Actions-International Reintegration Grants FP7-PEOPLE-2009-RG 256393 (to K.Y.), the

Yeda-Sela Center (to K.Y.), the Israel Cancer Research Foundation Postdoctoral Fellowship (to I.A.-D.), US National Institutes of Health (NIH) RO1CA126935 (to M.L.I.-A), T32HL069766 (training grant for T.T.C. and C.M.W.) and NIH HL049373 (to G.S.S.). S.A.F. is funded by the NIH (R56DK093399 and R01GM063904), the Carnegie Institution for Science endowment and the G. Harold and Leila Y. Mathers Charitable Foundation. B.M.W. is supported by the intramural program of the National Institute of Child Health and Human Development NIH, and by the Foundation Leducq.

References

1. Yaniv K, et al. Live imaging of lymphatic development in the zebrafish. Nat Med. 2006; 12:711–716. [PubMed: 16732279]
2. Lawson ND, Weinstein BM. In vivo imaging of embryonic vascular development using transgenic zebrafish. Dev Biol. 2002; 248:307–318. [PubMed: 12167406]
3. Hussain MM, et al. Microsomal triglyceride transfer protein in plasma and cellular lipid metabolism. Curr Opin Lipidol. 2008; 19:277–284. [PubMed: 18460919]
4. Raabe M, et al. Knockout of the abetalipoproteinemia gene in mice: reduced lipoprotein secretion in heterozygotes and embryonic lethality in homozygotes. Proc Natl Acad Sci U S A. 1998; 95:8686–8691. [PubMed: 9671739]
5. Marza E, et al. Developmental expression and nutritional regulation of a zebrafish gene homologous to mammalian microsomal triglyceride transfer protein large subunit. Dev Dyn. 2005; 232:506–518. [PubMed: 15614773]
6. Schlegel A, Stainier DY. Microsomal triglyceride transfer protein is required for yolk lipid utilization and absorption of dietary lipids in zebrafish larvae. Biochemistry. 2006; 45:15179–15187. [PubMed: 17176039]
7. Stoletov K, et al. Vascular lipid accumulation, lipoprotein oxidation, and macrophage lipid uptake in hypercholesterolemic zebrafish. Circ Res. 2009; 104:952–960. [PubMed: 19265037]
8. Schlegel A, Stainier DY. Lessons from “lower” organisms: what worms, flies, and zebrafish can teach us about human energy metabolism. PLoS Genet. 2007; 3:e199. [PubMed: 18081423]
9. Shelton JM, Lee MH, Richardson JA, Patel SB. Microsomal triglyceride transfer protein expression during mouse development. J Lipid Res. 2000; 41:532–537. [PubMed: 10744773]
10. Babin PJ, Gibbons GF. The evolution of plasma cholesterol: direct utility or a “spandrel” of hepatic lipid metabolism? Prog Lipid Res. 2009; 48:73–91. [PubMed: 19049814]
11. Babin PJ, et al. Both apolipoprotein E and A-I genes are present in a nonmammalian vertebrate and are highly expressed during embryonic development. Proc Natl Acad Sci U S A. 1997; 94:8622–8627. [PubMed: 9238027]
12. Thorpe JL, Doitsidou M, Ho SY, Raz E, Farber SA. Germ cell migration in zebrafish is dependent on HMGCoA reductase activity and prenylation. Dev Cell. 2004; 6:295–302. [PubMed: 14960282]
13. Amack JD, Yost HJ. The T box transcription factor no tail in ciliated cells controls zebrafish left-right asymmetry. Curr Biol. 2004; 14:685–690. [PubMed: 15084283]
14. Berriot-Varoqueaux N, Aggerbeck LP, Samson-Bouma M, Wetterau JR. The role of the microsomal triglygeride transfer protein in abetalipoproteinemia. Annu Rev Nutr. 2000; 20:663–697. [PubMed: 10940349]
15. Shoulders CC, et al. Abetalipoproteinemia is caused by defects of the gene encoding the 97 kDa subunit of a microsomal triglyceride transfer protein. Hum Mol Genet. 1993; 2:2109–2116. [PubMed: 8111381]
16. Rader DJ, Brewer HB Jr. Abetalipoproteinemia. New insights into lipoprotein assembly and vitamin E metabolism from a rare genetic disease. Jama. 1993; 270:865–869. [PubMed: 8340987]
17. Farber SA, et al. Genetic analysis of digestive physiology using fluorescent phospholipid reporters. Science. 2001; 292:1385–1388. [PubMed: 11359013]
18. Pickart MA, et al. Genome-wide reverse genetics framework to identify novel functions of the vertebrate secretome. PLoS One. 2006; 1:e104. [PubMed: 17218990]
19. Anderson JL, Carten JD, Farber SA. Zebrafish lipid metabolism: from mediating early patterning to the metabolism of dietary fat and cholesterol. Methods Cell Biol. 2011; 101:111–141. [PubMed: 21550441]

20. Breckenridge WC. Apolipoprotein C-II deficiency. Adv Exp Med Biol. 1986; 201:211–226. [PubMed: 3541516]
21. Hegele RA, et al. An apolipoprotein CII mutation, CIILys19----Thr' identified in patients with hyperlipidemia. Dis Markers. 1991; 9:73–80. [PubMed: 1782747]
22. Sethuraman G, et al. Familial homozygous hypercholesterolemia: report of two patients and review of the literature. Pediatr Dermatol. 2007; 24:230–234. [PubMed: 17542869]
23. Hegele RA. Plasma lipoproteins: genetic influences and clinical implications. Nat Rev Genet. 2009; 10:109–121. [PubMed: 19139765]
24. Connelly PW, Maguire GF, Little JA. Apolipoprotein CIISt. Michael. Familial apolipoprotein CII deficiency associated with premature vascular disease. J Clin Invest. 1987; 80:1597–1606. [PubMed: 3680515]
25. Landmesser U, Hornig B, Drexler H. Endothelial dysfunction in hypercholesterolemia: mechanisms, pathophysiological importance, and therapeutic interventions. Semin Thromb Hemost. 2000; 26:529–537. [PubMed: 11129409]
26. Henry PD. Hypercholesterolemia and angiogenesis. Am J Cardiol. 1993; 72:61C–64C.
27. Fazio S, Linton MF. Mouse models of hyperlipidemia and atherosclerosis. Front Biosci. 2001; 6:D515–525. [PubMed: 11229870]
28. Wouters K, Shiri-Sverdlov R, van Gorp PJ, van Bilsen M, Hofker MH. Understanding hyperlipidemia and atherosclerosis: lessons from genetically modified apoe and ldlr mice. Clin Chem Lab Med. 2005; 43:470–479. [PubMed: 15899668]
29. Hiratsuka S, Minowa O, Kuno J, Noda T, Shibuya M. Flt-1 lacking the tyrosine kinase domain is sufficient for normal development and angiogenesis in mice. Proc Natl Acad Sci U S A. 1998; 95:9349–9354. [PubMed: 9689083]
30. Kearney JB, et al. Vascular endothelial growth factor receptor Flt-1 negatively regulates developmental blood vessel formation by modulating endothelial cell division. Blood. 2002; 99:2397–2407. [PubMed: 11895772]
31. Chappell JC, Taylor SM, Ferrara N, Bautch VL. Local guidance of emerging vessel sprouts requires soluble Flt-1. Dev Cell. 2009; 17:377–386. [PubMed: 19758562]
32. Bussmann J, et al. Arteries provide essential guidance cues for lymphatic endothelial cells in the zebrafish trunk. Development. 2010; 137:2653–2657. [PubMed: 20610484]
33. Shelness GS, Hou L, Ledford AS, Parks JS, Weinberg RB. Identification of the lipoprotein initiating domain of apolipoprotein B. J Biol Chem. 2003; 278:44702–44707. [PubMed: 12941937]
34. Hessler JR, Robertson AL Jr, Chisolm GM 3rd. LDL-induced cytotoxicity and its inhibition by HDL in human vascular smooth muscle and endothelial cells in culture. Atherosclerosis. 1979; 32:213–229. [PubMed: 223585]
35. Usui R, Shibuya M, Ishibashi S, Maru Y. Ligand-independent activation of vascular endothelial growth factor receptor 1 by low-density lipoprotein. EMBO Rep. 2007; 8:1155–1161. [PubMed: 17962812]
36. Yla-Herttuala S, Alitalo K. On the relationship of LDL and VEGFR1: not just a family affair. EMBO Rep. 2007; 8:1127–1128. [PubMed: 18059310]
37. Arany Z, et al. HIF-independent regulation of VEGF and angiogenesis by the transcriptional coactivator PGC-1alpha. Nature. 2008; 451:1008–1012. [PubMed: 18288196]
38. Fraisl P, Baes M, Carmeliet P. Hungry for blood vessels: linking metabolism and angiogenesis. Dev Cell. 2008; 14:313–314. [PubMed: 18331707]
39. Hagberg CE, et al. Vascular endothelial growth factor B controls endothelial fatty acid uptake. Nature. 2010; 464:917–921. [PubMed: 20228789]
40. Isogai S, Lawson ND, Torrealday S, Horiguchi M, Weinstein BM. Angiogenic network formation in the developing vertebrate trunk. Development. 2003; 130:5281–5290. [PubMed: 12954720]
41. Roman BL, et al. Disruption of acvrl1 increases endothelial cell number in zebrafish cranial vessels. Development. 2002; 129:3009–3019. [PubMed: 12050147]
42. Isogai S, Horiguchi M, Weinstein BM. The vascular anatomy of the developing zebrafish: an atlas of embryonic and early larval development. Dev Biol. 2001; 230:278–301. [PubMed: 11161578]

43. Shireman R, Kilgore LL, Fisher WR. Solubilization of apolipoprotein B and its specific binding by the cellular receptor for low density lipoprotein. Proc Natl Acad Sci U S A. 1977; 74:5150–5154. [PubMed: 200946]
44. Nicoli S, De Sena G, Presta M. Fibroblast Growth Factor 2-induced angiogenesis in zebrafish: the zebrafish yolk membrane (ZFYM) angiogenesis assay. J Cell Mol Med. 2008
45. Habeck H, Odenthal J, Walderich B, Maischein H, Schulte-Merker S. Analysis of a zebrafish VEGF receptor mutant reveals specific disruption of angiogenesis. Curr Biol. 2002; 12:1405–1412. [PubMed: 12194822]
46. Bligh EG, Dyer WJ. A rapid method of total lipid extraction and purification. Can J Biochem Physiol. 1959; 37:911–917. [PubMed: 13671378]
47. Itkin M, et al. GLYCOALKALOID METABOLISM1 is required for steroidal alkaloid glycosylation and prevention of phytotoxicity in tomato. Plant Cell. 2011; 23:4507–4525. [PubMed: 22180624]
48. Pham VN, et al. Combinatorial function of ETS transcription factors in the developing vasculature. Dev Biol. 2007; 303:772–783. [PubMed: 17125762]
49. Takada N, Appel B. Identification of genes expressed by zebrafish oligodendrocytes using a differential microarray screen. Dev Dyn. 2010; 239:2041–2047. [PubMed: 20549738]
50. Zygmunt T, et al. Semaphorin-PlexinD1 signaling limits angiogenic potential via the VEGF decoy receptor sFlt1. Dev Cell. 2011; 21:301–314. [PubMed: 21802375]
51. Hansen MB, Nielsen SE, Berg K. Re-examination and further development of a precise and rapid dye method for measuring cell growth/cell kill. J Immunol Methods. 1989; 119:203–210. [PubMed: 2470825]
52. Sellers JA, Hou L, Athar H, Hussain MM, Shelness GS. A Drosophila microsomal triglyceride transfer protein homolog promotes the assembly and secretion of human apolipoprotein B. Implications for human and insect transport and metabolism. J Biol Chem. 2003; 278:20367–20373. [PubMed: 12657646]
53. Gore AV, Lampugnani MG, Dye L, Dejana E, Weinstein BM. Combinatorial interaction between CCM pathway genes precipitates hemorrhagic stroke. Dis Model Mech. 2008; 1:275–281. [PubMed: 19093037]

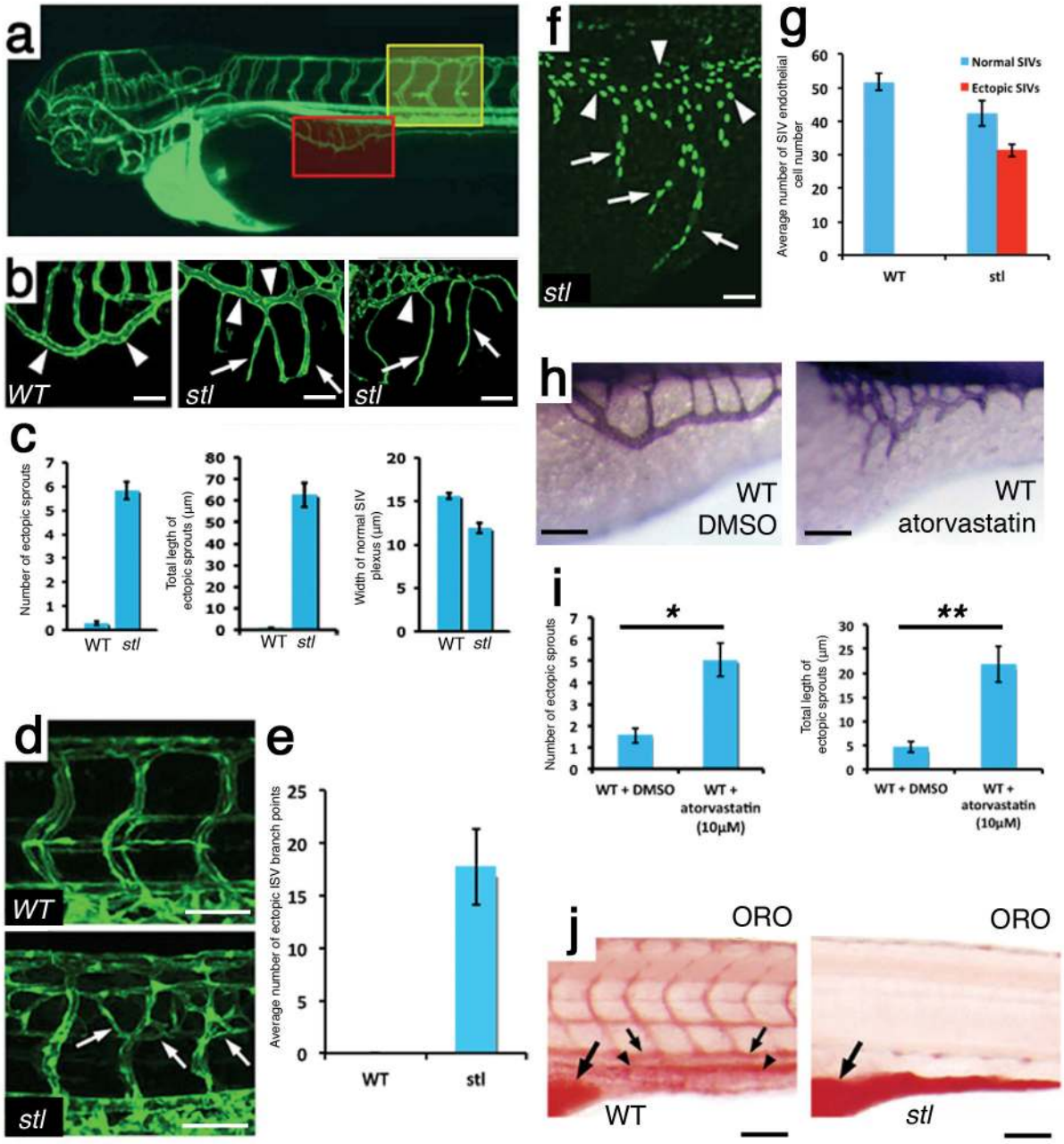

Figure 1.

stl is a zebrafish mutant with excessive angiogenesis. (**a**) Confocal angiography of a 3.5-dpf zebrafish illustrating the SIVs (boxed in red) and the ISVs (boxed in yellow). (**b**) Confocal images of SIVs (shown boxed in red in **a**) in 3.5-dpf WT *Tg(fli1:eGFP)*^{y1} (right) and 3.5-dpf and 5-dpf *stl* mutant larvae (middle and left, respectively). Ectopic segments (arrows) extend from the subintestinal vein (arrowheads). (**c**) Quantification of the ectopic sprouting phenotype is *stl* mutants (n_{WT} = 87, n_{stl} = 107). (**d**) Confocal images of ISVs (shown boxed in yellow in **a**) in the midtrunks of 5-dpf *Tg(fli1:eGFP)*^{y1} WT (top) and *stl* mutant (bottom) larvae. Ectopic sprouts in the *stl* mutants are indicated with arrows. (**e**) Quantification of the average number of ectopic ISV branch points in WT larvae and *stl* mutants (n_{WT} = 16, n_{stl} = 27). (**f**) Confocal image of SIVs in a 3.5-dpf *stl; Tg(fli1:neGFP)*^{y7} zebrafish with the

endothelial cell nuclei visible in the normal plexus (arrowheads) and in ectopic sprouts (arrows). (**g**) Quantification of the average number of endothelial cell nuclei in the yolk area of WT and *stl* mutant larvae ($n_{WT} = 12$, $n_{stl} = 14$). $P = 7.3 \times 10^{-6}$ by *t* test. (**h**) Alkaline phosphatase staining of SIVs in WT larvae treated with DMSO (left) or atorvastatin (right). (**i**) Quantification of the average number (left) ($n_{WT+DMSO} = 41$, $n_{WT+atorvastatin} = 38$) and average total length (right) ($n_{WT+DMSO} = 39$, $n_{WT+atorvastatin} = 35$) of ectopic SIV segments. $^{*}P = 1.4 \times 10^{-4}$, $^{**}P = 7.7 \times 10^{-5}$ by *t* test. (**j**) Transmitted light images of 5-dpf ORO-stained WT (left) and *stl* mutant (right) larvae. The yolk is indicated by large arrows. The main vessels are indicated by small arrows and arrowheads. Scale bars, **b**, **f**, **h** and **j**, 30 μm; **d**, 60 μm. All values are mean ± s.e.m

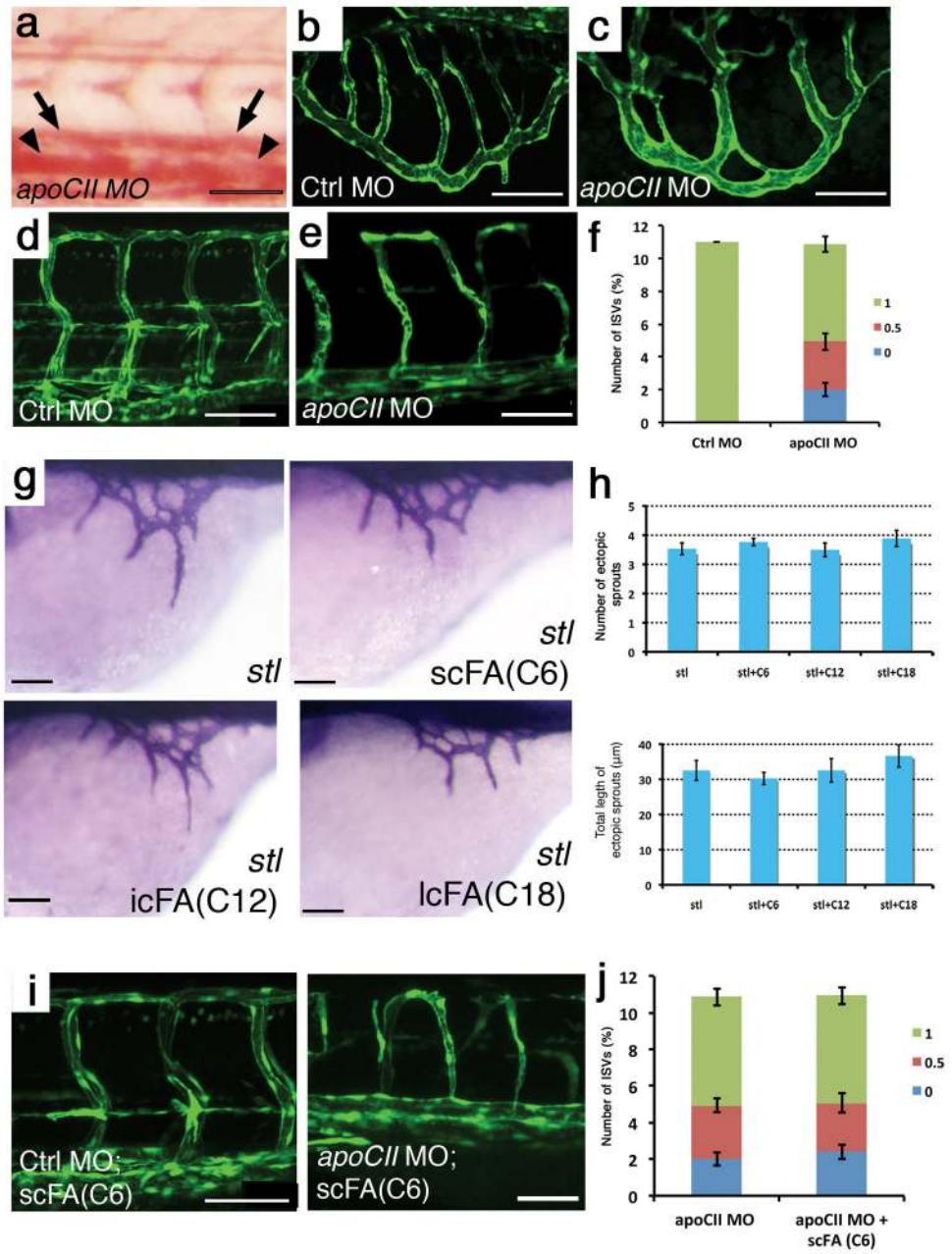

Figure 2.

The excessive angiogenesis phenotype is not caused by global lipid starvation. (**a**) Transmitted light image of a 4-dpf ORO-stained larva injected with *apoCII* morpholino oligonucleotides (MOs). The dorsal aorta and the cardinal vein are indicated by arrows and arrowheads, respectively. (**b**–**e**) Confocal imaging of SIVs (**b**, **c**) and ISVs (**d**, **e**) in 3.5-dpf *Tg(fli1:eGFP)*^{y1} larvae injected with a control morpholino oligonucleotide (ctrl) (**b**, **d**) or an *apoCII* morpholino oligonucleotide (**c**, **e**). (**f**) Quantification of the ISV phenotypes of control (n=17) or *apoCII* morpholino-oligonucleotides–injected (n=15) zebrafish embryos. The bars show the percentages of ISVs that have failed to sprout (0, blue), ISVs that have grown only up to the horizontal myoseptum half way up the trunk (0.5, red) and ISVs that have grown all the way to the dorsal trunk to form the Dorso-Lateral Anastomotic Vessel (1,

green). (**g**) Alkaline phosphatase staining of SIVs in 3.5-dpf *stl* mutants either not treated (left, top) or treated with short-chain fatty acids (C_6) (scFA) (right, top), intermediate-chain fatty acids (C_{12}) (icFA) (left, bottom) or long-chain fatty acids (C_{18}) (lcFA) (right, bottom). (**h**) Quantification of the ectopic sprouting phenotype. *stl*, untreated *stl* mutants; *stl*+C_6, *stl* mutants plus short-chain fatty acids; *stl*+C_{12}, *stl* mutants plus intermediate-chain fatty acids; *stl*+C_{18}, *stl* mutants plus long-chain fatty acids. $n_{control} = 27$, $n_{C6} = 29$, $n_{C12} = 21$, $n_{C18} = 17$. **P* (top) = 0.517, ***P* (bottom)= 0.5058 by analysis of variance. (**i**) Confocal images of trunk ISVs in embryos injected with control morpholino oligonucleotides (left) or *apoCII* morpholino oligonucleotides (right) and treated with short-chain fatty acids. (**j**) Quantification of the phenotype of trunk ISVs in embryos injected with *apoCII* morpholino oligonucleotides that were soaked either in normal medium ($n = 15$) or in medium supplemented with short-chain fatty acids ($n = 17$). Trunk ISVs were classified as in **f**. $P = 0.839$ by χ^2 test for injection of *apoCII* morpholino oligonucleotides compared to *apoCII* morpholino oligonucleotides plus short-chain fatty acids. Scale bars, **a**, **b**, **c** and **g**, 30 μm; **d**, **e** and **i**, 60 μm. Data in (**f, h, j**) are mean ± s.e.m.

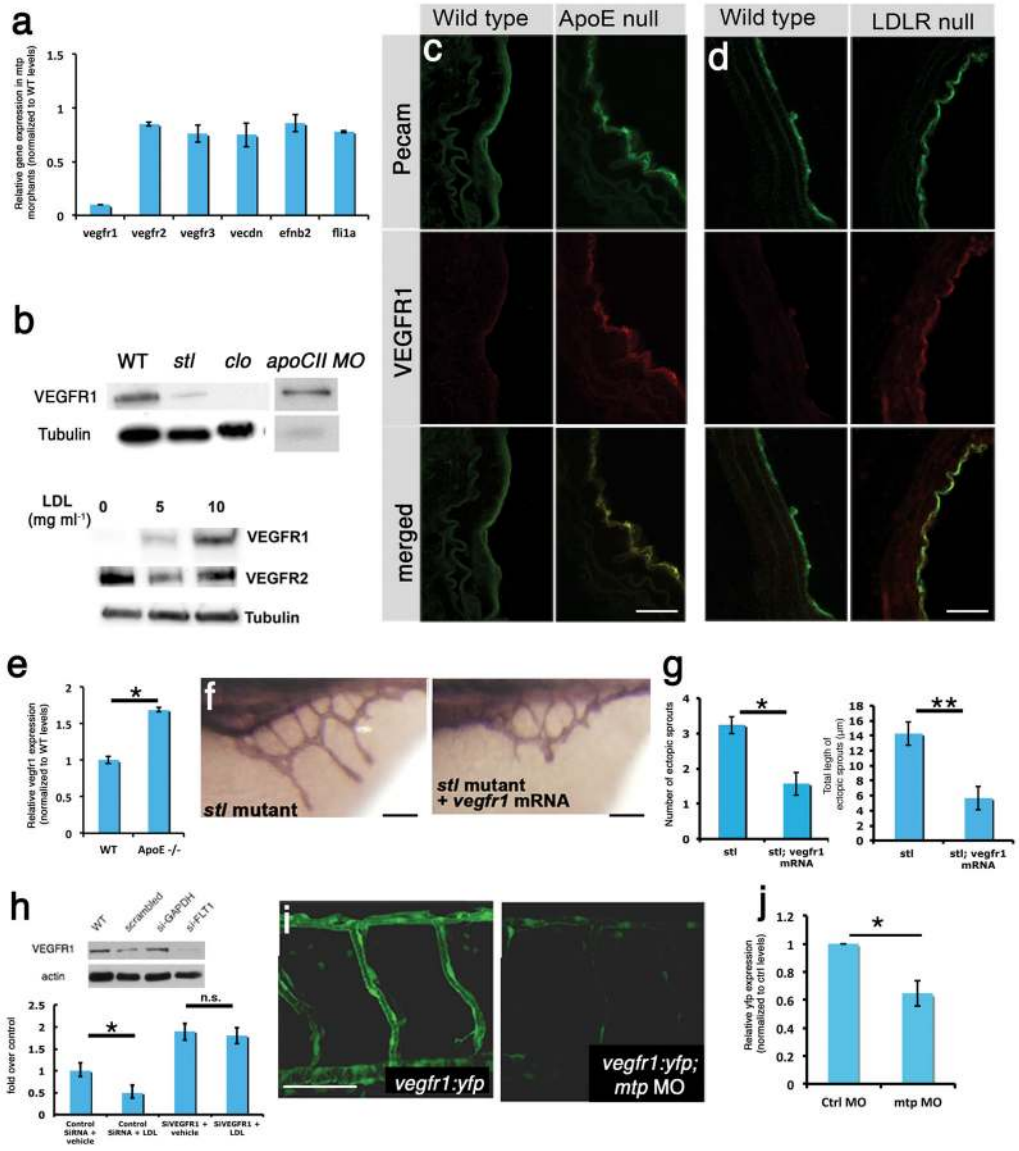

Figure 3.

Lipoprotein concentrations regulate the expression of VEGFR1. (**a**) The expression of the indicated mRNAs in 24-hpf embryos injected with *mtp* morpholino oligonucleotides (MO) ($n_{\text{control MO}} = 50$, $n_{mtp\ \text{MO}} = 30$). (**b**) Western blots detecting VEGFR1 and tubulin in extracts from 3-dpf zebrafish (top) ($n_{\text{control MO}} = 30$, $n_{apoCII\ \text{MO}} = 30$, $n_{stl} = 30$, $n_{clo} = 20$). Western blots detecting VEGFR1, VEGFR2 and tubulin in lysates from HUVECs cultured in LDL^{-} media with or without the addition of LDL (bottom). The data shown are representative of 3 independent experiments. (**c**, **d**) Confocal images of aortic roots in WT C57BL/6 (left, **c**) and *Apoe*-null (right, **c**) littermates and of abdominal aortas in WT C57BL/6 (left, **d**) and *Ldlr*-null (right, **d**) littermates stained with Pecam-specific (top) or VEGFR1-specific (middle) antibodies. Merged images are presented at the bottom. Scale bars, 25 μm. (**e**) Semiquantitative RT-PCR measurement of *Vegfr1* mRNA expression in aortic arches dissected from WT ($n = 5$) and *Apoe*-null ($n = 5$) mice. *$P = 4 \times 10^{-14}$ by z test. (**f**) Transmitted light images of alkaline-phosphatase–stained SIVs in a 3.5-dpf *stl* mutant not injected (left) or injected with *vegfr1* mRNA (right). (**g**) Quantification of the

ectopic sprouting phenotype (n_{stl} = 26, $n_{stl+vegfr1\ \mathrm{mRNA}}$ = 23). *P = 1.6 × 10^{-4}, **P = 2.6 × 10^{-4} by t test. (**h**) Western blots detecting VEGFR1 and actin in lysates from HUVECs exposed to the indicated siRNAs (top). siGAPDH, siRNA targeting glyceraldehyde-3-phosphate dehydrogenase (GAPDH); siVEGFR1, siRNA targeting VEGFR1. Migration area of HUVECs treated with either LDL or vehicle as a response to a 200-μm wound (bottom). Bars represent mean ± s.e.m. (**i**) Confocal images of *Tg(flt1:YFP)*^{hu4624} (left) and *mtp* morpholino-oligonucleotide–injected *Tg(flt1:YFP)*^{hu4624} (right) embryos. (**j**) *yfp* mRNA expression levels in 48-hpf WT and *mtp* morpholino-oligonucleotide–injected *Tg(flt1:YFP)*$^{hu4624/+}$ embryos ($n_{Tg(flt1:YFP)hu4624}$ = 98, $n_{Tg(flt1:YFP)hu4624\ +\ mtp\ MO}$= 73) *$P$ = 0.0248 by t test. Scale bar in **f**, 30μm; **i**, 60 μm. NS, not significant. All data (**a, e, g, h, j**) are mean ± s.e.m.

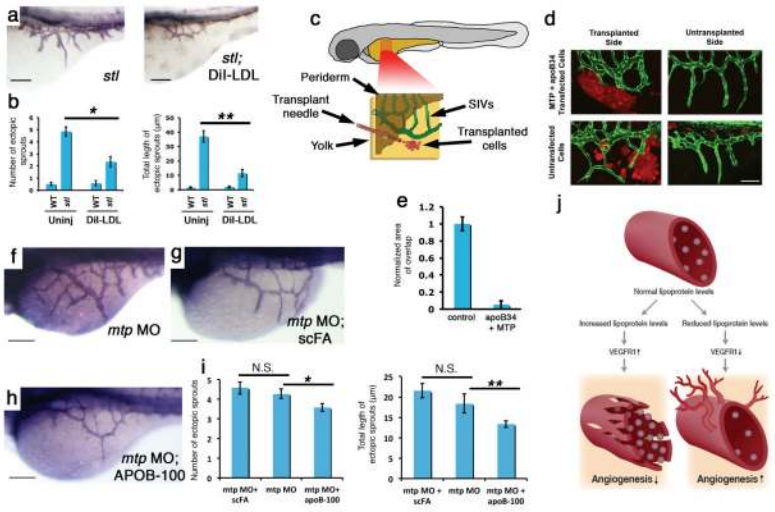

Figure 4.

ApoB particles regulate angiogenesis by directly acting on endothelial cells. (**a**) Alkaline phosphatase staining of SIVs of 3.5-dpf *stl* mutants either not injected (right) ($n = 26$) or injected intravascularly with DiI-LDL (left) ($n = 14$). (**b**) Quantification of the ectopic sprouting phenotype. *$P = 0.0001$, **$P = 0.75$ by *t* test. Uninj, uninjected. (**c**) Diagram illustrating the procedure used for transplanting lipoprotein-secreting HEK293 cells into the yolk area of zebrafish embryos. (**d**) Confocal images of the SIVs (green) of 3.5-dpf *Tg(fli1:eGFP)*^{y1} zebrafish transplanted with HEK293 cells transfected with plasmids encoding MTP and ApoB34 (top; $n = 3$) or with untransfected control cells (bottom; $n = 3$) (red) on one side of the yolk ball. Untransplanted (right) and transplanted (left) sides of the same embryo are shown. (**e**) Quantification of the area of overlap between the SIV endothelium and HEK293 cells in 3.5-dpf transplanted zebrafish, normalized to the total length of the interface between the two cell populations. (**f–h**) Alkaline phosphatase staining of SIVs of 4.5-dpf *stl* mutants either not injected ($n = 16$) (**f**) or injected intravascularly with short chain fatty acid ($n = 10$) (**g**) or a delipidated form of ApoB-100 ($n = 24$) (**h**). (**i**) Quantification of the ectopic sprouting phenotype. *$P = 0.0411$, **$P = 4.6 \times 10^{-5}$ by *t* test. (**j**) Schematic model illustrating the effects of circulating ApoB-containing lipoproteins on angiogenesis. Scale bars, **a**, **f–h**, 30 μm; **d**, 60 μm. NS, not significant. Data in (**b, e, i**) are mean ± s.e.m.